

# Searching for heavy charged Higgs bosons in the neutrino{tau decay mode at LHC

Kosuke Odagiri

Rutherford Appleton Laboratory,  
Chilton, Didcot, Oxford OX11 0QX, UK.

## Abstract

We discuss the search for the heavy charged Higgs bosons  $H^\pm$ , implicitly of the Minimal Supersymmetric Standard Model, in the  $\tau$  decay mode at the LHC. Compared to the dominant decay mode  $H^\pm \rightarrow b\bar{t}$ , the channel suffers from suppression due to the branching ratio and the lack of direct mass reconstruction, but the reduced QCD background makes it a feasible channel especially in the large  $\tan\beta$  region. We study the production in  $b\bar{t}$  fusion via  $b\bar{t}H^\pm \rightarrow \tau^\pm \bar{\nu}_\tau H^\pm$ , and the leading irreducible background  $b\bar{t} \rightarrow \tau^\pm \bar{\nu}_\tau$ . Our results indicate that for the  $H^\pm$  mass of greater than 200 GeV and up to 1 TeV and higher, they can be discovered in this channel for a vast range of the parameter space, down to at least  $\tan\beta \approx 3$  and potentially the whole range of  $\tan\beta$  down to 1.5 if the signal selection efficiency could be improved fourfold. Our analysis is sensitive to top quark identification at large rapidity, and should be supplemented with a full study including jet showering and detector effects.

# 1 Introduction

The charged Higgs bosons  $H^\pm$  are a central prediction of the Two Higgs Doublet Model which is necessitated by supersymmetry. Given the results of recent experimental analyses, the neutral Higgs exclusion at LEP 2 [1] and the constraint on the rare bottom quark decay  $b \rightarrow s \gamma$  [2], both of which favour the elusive heavy mass region for  $H^\pm$ , at least in the MSSM, it is important to establish the parameter regions in which  $H^\pm$  can be discovered at present and future colliders.

It is believed [3] that LEP 2 can not discover the charged Higgs bosons in the mass regions indicated by the Minimal Supersymmetric Standard Model (MSSM) and the current bound [1] on neutral Higgs bosons, viz the mass relation  $M_H^2 = M_W^2 + M_{A_0}^2 \approx 110$  GeV. The search for such a particle needs greater centre-of-mass energy, notably at LHC and, to a more limited extent, Tevatron [4]. The purpose of this paper is to establish the significance of the secondary  $H^\pm$  decay channels, mainly at LHC.

If  $H^\pm$  are 'heavy', which is taken from here on to imply  $M_{H^\pm} \gtrsim m_t$ , they can not be produced in top decay and the main production mode for them at hadron colliders is 'bt fusion', viz:

$$gb \rightarrow tH^\pm \rightarrow t\bar{t} + H^\pm \quad (1)$$

We have taken  $b$  as a sea quark, as is appropriate at such high energy collisions, whereas  $t$  is created via  $g \rightarrow t\bar{t}$ . Of course the charge conjugate process  $gb \rightarrow tH^+ \rightarrow t\bar{t} + H^+$  must also be included, and this behaves in exactly the same way since there is no intrinsic  $b$  component of the proton.

The above production channel has been studied extensively in the literature [5]. Recent analyses have focussed on the dominant decay mode  $H^\pm \rightarrow tb$  and the reduction of the QCD background associated with it. The utilisation of the less dominant decay modes was discussed in the past [6]. Here we focus on the decay mode  $H^\pm \rightarrow t\bar{t} + H^\pm$ , improving on previous analyses, partly by adopting the latest numbers for Standard Model parameters and parton distribution functions, but mainly by a new set of kinematic selection techniques to reduce the background. Any excess over the background so observed can be considered as due to  $H^\pm$  by applying the tau polarisation analysis [7].

The result of our analysis indicates that the discovery region for  $H^\pm$  is far greater than has previously been thought, covering the whole of the  $(M_{H^\pm}, \tan \beta)$  parameter space up to  $M_{H^\pm} \approx 1$  TeV and higher, and down to at least  $\tan \beta \approx 3$ . Optimisation in the analysis procedure and parameters can potentially extend the lower limit in  $\tan \beta$  to 1.5, below which is excluded by LEP 2 measurements so far in the MSSM.

# 2 Calculation

In order to minimise the parameter dependence of our calculations and to make them applicable to as wide a range of parameters as possible, we adopt  $M_{H^\pm}$  and  $\tan \beta$  as the two Higgs sector parameters. When considering the  $H^\pm$  decays, let us furthermore assume that the neutral Higgs mixing angle  $\theta_W$  is given by  $\theta_W = \beta = 2^\circ$  which holds in MSSM at tree level in the heavy mass limit of the charged Higgs bosons, explicitly,  $M_{H^\pm}^2 = M_Z^2$ . In this limit, practically the only Standard Model decay modes are  $tb$  and  $t\bar{t}$ , and we assume superpartners too heavy to be produced in  $H^\pm$  decays.

We restrict our discussions to the tree level, since our primary purpose is to establish the plausibility of signal detection, rather than to propose precision measurements. We adopt MRS 1998 leading order parton distributions [8], and calculate the strong coupling at one loop using the default MRS parameter values, neglecting virtual top contributions in both cases.

We assume zero kinematic bottom quark mass to be consistent with the sea quark picture we are adopting, whereas we retain finite bottom quark pole mass  $m_b$  for the Yukawa coupling, which we take to be 4.25 GeV. Similarly, we take the tau kinematic mass to be zero and set the Yukawa coupling mass to 1.78 GeV. Both kinematic and Yukawa masses of the top quark are taken to be 175 GeV. The top quark,  $H^+$  and  $W$  widths are calculated at tree level, although we adopt the narrow width approximation for the top quark and  $H^+$ . We also note that the quark masses implicit in the parton distribution functions are independent parameters which are in general distinct from the kinematic and Yukawa masses we choose to adopt.

The electroweak parameters are  $e_M = 1 = 128$ ,  $\sin^2 \theta_W = 0.2315$ ,  $M_Z = 91.187$  GeV,  $M_W = M_Z \cos \theta_W = 79.94$  GeV. The Cabibbo-Kobayashi-Maskawa matrix element  $V_{CKM}^2$  [9] is taken to be 1 (it is practically 1. See [9]).

As for the LHC collider parameters [10], the centre-of-mass energy for  $pp$  collision is 14 TeV. Integrated luminosities of  $10 \text{ fb}^{-1}$  and  $100 \text{ fb}^{-1}$  per year are expected in the low luminosity and high luminosity options, respectively.

The squared matrix elements are calculated by hand with the usual trace method, convoluted with the MRS parton distribution functions, and integrated using VEGAS [11]. The results are tested against the literature [6] where they are available, and tests of gauge independence were carried out by hand.

When computing decay level distributions, the top quark is assumed to be on the mass shell using the so-called 'narrow width approximation', in order to minimise the number of 'unphysical' Feynman graphs we must consider without violating gauge invariance. We similarly take the  $W$  boson arising from top quark decay to be on shell.

For the signal events, we assume that the top quark decays independently of production, by neglecting the spin correlation effects which are anyhow small for our purposes, in order to maximise the parameter space that can be covered in our analysis. Since we take top quark to be on the mass shell, this procedure is exact in the limit of identical left and right  $H^+$  coupling, at  $\tan \beta = m_t = m_b$ . We also take  $H^+$  to be on the mass shell since we do not consider the finite width effect to be important at this stage.

For the background we incorporate the exact decay distribution of the top quark, and the finite constant width of  $W$ , both of which are potentially important when considering kinematic cuts to reduce the background. The calculation was tested using FORM [12].

The theoretical uncertainties associated with the above procedure are expected to be dominated by two sources. Firstly, the QCD higher order corrections which are of the order  $\alpha_s(M_H) \approx 10\%$ . To be more precise, our procedure will need to be tested for jet and detector effects, which must be carried out using Monte Carlo simulations where the leading QCD corrections are resummed and factorised. Secondly, as we discuss in the next chapter, the possibility of the other decay modes, such as the  $H^+ \rightarrow hW$  decay mode for relatively light  $H^+$  at low  $\tan \beta$ .

### 3 Analysis strategy

The tree level Feynman diagrams for the signal process are shown in figure 1. The spin- and colour-averaged matrix element squared for the process simplifies as follows:

$$\overline{M}^2 (g_{(1)} b_{(2)} \bar{t} t_{(3)} H_{(4)}) = \frac{g_s^2}{2N_c} \frac{e^2}{2 \sin^2 w} \frac{m_b^2 \tan^2 + m_t^2 \cot^2}{2M_w^2} \frac{u_4^2}{s t_3} \frac{1 + 2 \frac{m_4^2}{u_4} \frac{m_3^2}{m_t^2}}{1 + \frac{m_3^2}{t_3} + \frac{m_4^2}{u_4}} : \quad (2)$$

Here  $g_s$  is the strong coupling,  $g_s^2 = 4 = \alpha_s$ , and as a first approximation we evaluate it at scale  $Q = (m_3 + m_4)$ .  $N_c = 3$  for QCD.  $s, t$  and  $u$  are the usual Mandelstam variables, defined with the partonic momenta.  $t_3 = t - m_3^2 = t - m_t^2$  and  $u_4 = u - m_4^2 = u - M_H^2$ .  $\tan w$  is the ratio of the two expectation values of the two Higgs doublets, and we assume  $1 < \tan w < m_t = m_b$ .

We do not tag the spectator bottom quark. However, in order to reduce the background, for example, from top pair,  $W$  pair and single  $W$  production, and to have a grip on the irreducible background, we do make use of the 'spectator' top quark,  $t_{(3)}$ . In [6, 13], the following 'stri lepton' procedure was proposed: the top quark moves nearly parallel to the original  $g_{(1)}$  parton direction, and will be lost in the beam jets. However, if it decays leptonically, the electron or muon will be kicked out with  $p_T$  of the order  $m_t = 2$  so that this can be used to trigger the signal events. Potentially the bottom quark can also be tagged, especially when it decays leptonically.

In this study we consider both the leptonic and hadronic decays. Although the leptonic mode is more inclusive, the hadronic branching fraction is larger ( $BR[\text{hadronic}] = 2/3$ ), and the lack of the missing momentum from leptonic decay makes the handling of the kinematic distributions more transparent.

In the leptonic decay mode, we consider the inclusive sample of top-like events, wherein we assume the top quark identification to be carried out with a universality of "t", with " $t$ "  $BR[\text{leptonic}] = 2/9$ .

In the hadronic decay mode, we require the inclusive multi-jet final state to have a reconstructed mass near the top mass. If bottom jet tagging can be utilised, this will aid the procedure by allowing the  $W$  mass to be reconstructed also. We can not make a full simulation of the top quark identification efficiency, but as a first approximation we require all parton level decay products to be reasonably away from the beam directions, at pseudorapidities of less than 1.5 in order to reduce the QCD noise. We do not impose cuts on separation between top decay products.

It has been shown [13], and we will assume, that the tagging of the top quark is very effective in reducing the background, eliminating all but the irreducible background:

$$gb \bar{t} tW ; \quad (3)$$

whose presence is the main obstacle to the observation of the signal (1).

Let us assume the leptonic decay mode  $H \rightarrow t \bar{t}$ . In the limit of heavy  $H$ ,  $M_H^2 \gg m_t^2$ , the branching ratio is easily seen to be given by:

$$BR[t \bar{t}] = \frac{[t \bar{t}]}{[bt]} = \frac{m^2 \tan^2}{N_c (m_t^2 \cot^2 + m_b^2 \tan^2)} : \quad (4)$$

For finite  $M_H$  the branching ratio is always greater than this limit, as there is kinematic suppression on top quark for the  $H \rightarrow b\bar{b}$  decay mode, which goes as  $(1 - m_t^2/M_H^2)$ . Thus if there are no other decay modes:

$$BR[H \rightarrow b\bar{b}] = 1 + \frac{m_b^2 N_C}{m^2} \left( 1 + \frac{m_t^2}{m_b^2 \tan^4} \right) \left( 1 - \frac{m_t^2}{M_H^2} \right)^{-1} : \quad (5)$$

Figure 2a shows the  $M_H^2 - m_t^2$  limit of equation (5), as a function of  $\tan \alpha$ . By requiring the other decay modes to vanish, we have implicitly assumed  $\cos^2(\alpha) = 0$  which holds in the heavy mass limit in the MSSM at tree level. The  $H \rightarrow W^+ W^- h^0$  decay rate is proportional to this. The ratio of this mode to the  $b\bar{b}$  mode is given by:

$$\frac{W^+ W^- h^0}{b\bar{b}} = \frac{3=2 M_H ; M_W ; M_{h^0} \cos^2(\alpha)}{2N_C 1=2 M_H ; m_t ; 0 M_H^2 (m_b^2 \tan^2 + m_t^2 \cot^2)} \quad (6)$$

where  $[m_1; m_2; m_3] = (m_1^2 - (m_2 + m_3)^2)(m_1^2 - (m_2 - m_3)^2)$  and is symmetric under the permutations of the three masses. At tree level in MSSM, it can be shown that  $\cos^2(\alpha)$  is given in terms of the pseudoscalar Higgs mass  $M_A$  and  $\tan \alpha$  by:

$$\cos^2(\alpha) = \frac{1}{2} \frac{M_A^2 \sin 4\alpha}{M_A^2 + M_Z^2 \cos 4\alpha} \quad (7)$$

Combined with equation (6), the approximation is valid if  $M_A^2 \ll M_Z^2$  which is implicit in  $M_H^2 \gg m_t^2$  since  $M_H > M_A$  in MSSM. However, if  $m_t + m_b > M_W + M_{h^0}$ , the  $W^+ W^- h^0$  decay could dominate in a small window, noting  $M_{h^0} \approx 80$  GeV, just below the threshold for the  $b\bar{b}$  mode.

The factor  $(m_t^2 \cot^2 + m_b^2 \tan^2)$  cancels between (2) and (4), and we see that the cross section relevant to us goes as:

$$\overline{M} \overline{f}(gb \rightarrow tH \rightarrow t\bar{t}) / \frac{m^2 \tan^2}{2N_C M_W^2} : \quad (8)$$

In figure 2(b) we plot this quantity, which represents the overall  $\tan \alpha$  dependence of production and decay in the  $t\bar{t}$  mode. The  $1=BR[H \rightarrow b\bar{b}]$  contribution, neglected in (4) and (8), is also included in this plot. In addition, in our forthcoming simulations in the next chapter, we also include the kinematic  $(1 - m_t^2/M_H^2)$  suppression on the  $b\bar{b}$  decay mode.

The complete matrix element squared for the background process (3), including the  $t\bar{t}$  and  $W^+ W^-$  decay, is available in [14]. However, in order to gain insight into the structure of the background process let us present the spin- and colour-averaged matrix element squared for (3). The Feynman graphs are identical to figure 1 with the substitution  $H \rightarrow W^+ W^-$ , in the following simple form<sup>1</sup>:

$$\overline{M} \overline{f}(g_{(1)} b_{(2)} \rightarrow t_{(3)} W_{(4)}) = \frac{g_s^2}{2N_C} \frac{e^2}{2 \sin^2 \theta_W} \frac{1}{2 + 1 + \frac{m_3^2}{2m_4^2}} \frac{\frac{u_4^2}{st_3}}{1 + 2 \frac{m_4^2 - m_3^2}{u_4}} \frac{1 + \frac{m_3^2}{t_3} + \frac{m_4^2}{u_4}}{1 + \frac{m_3^2}{t_3} + \frac{m_4^2}{u_4}} \quad (9)$$

<sup>1</sup> In our decay level simulations we supplement (9) by including the top quark and  $W^+ W^-$  decay, with the top quark being on shell, as well as the  $W^+$  from top quark decay. For the signal, (2) is supplemented similarly, but we set the  $H$  on shell, and assume the top quark to decay independently of production by averaging over the top quark helicities, as mentioned in the previous chapter. Neither of these approximations are expected to have a significant effect on our results.

This contains an 'isotropic' part, the 2 inside the first square brackets, and a 'scalar' part whose kinematics are exactly proportional to the signal cross section (2) in the limit of degenerate  $H$  and  $W$  masses. The ratio of the two is around 1:1 (see forthcoming table 1). As for the  $W$  branching ratio into  $\tau^+ \tau^-$ , this equals 1=9 11%. Thus in this limit, the ratio of signal to non-isotropic, 'scalar' background, assuming  $H$  branching ratio of equation (4), is:

$$\frac{(gb \tau^+ \tau^- ! t \tau^+ \tau^-)}{(gb \tau^+ \tau^- ! t \tau^+ \tau^-)_{\text{scalar}}} = \frac{9}{2N_c} \frac{m \tan \theta}{M_W} \frac{2}{m_t^2 + 2M_W^2} : \quad (10)$$

$M_W = m_t = 40$ , so this amounts to some excess of signal over background for large values of  $\tan \theta$ . In reality, this will be reduced further by the phase space suppression on  $H$  production, but to compensate for this, the mass difference between  $H$  and  $W$  can be exploited in kinematic cuts. A more subtle point is that  $H$  are scalar whereas  $W$  are vector, leading to different distributions of the decay products which may be utilised once a significant excess of signal over background is observed through the kinematic cuts. As a final stage of the signal/background analysis, we can use tau polarisation as described in [7], noting that their helicities are predominantly left in  $W$  decay, whereas they are predominantly right in  $H$  decay.

To summarise, our strategy is as follows. Firstly, we select events with top quarks, possibly identified using the single lepton trigger, of the form  $s t^+ t^- + E_T + X$  in the hadronic top quark decay mode, or  $e^+ e^- + E_T + X$  in the leptonic decay mode, where  $e$  is  $e$  or  $\mu$ ,  $E_T$  is the typically large missing transverse energy, and  $X$  contains jets near the beam directions. Secondly, we utilise kinematic cuts to screen out  $W$  events. At this stage, it is desirable to be able to reconstruct the  $H$  mass from the transverse momentum distribution of tau. In experimental analyses, the kinematic selection cuts will be replaced by the fitting of the distributions with signal and background expectations, which is a more elegant and effective procedure. Thirdly, we apply tau polarisation and spin correlation analyses in order to confirm the presence of  $H$ .

## 4 Results

The total signal cross section, corresponding to (1) but excluding the  $\tan \theta$  dependence of equation (8), the kinematic suppression on the mode of equation (4), and excluding the bg initial state and the charge conjugate processes, is shown in figure 3. It can be seen that the cross section falls approximately exponentially with increasing  $M_H$ , but even for large masses the cross section is significant, bearing in mind the integrated luminosity of  $100 \text{ fb}^{-1}$  per year in the high luminosity option at LHC.

In table 1 we present the typical signal and background cross sections including the  $\tan \theta$  dependence, the kinematic suppression on the mode, factor 4 for the bg initial state and charge conjugation, and the  $W \rightarrow \tau^+ \tau^-$  branching ratio of 1/9. It is clear that the signal suffers from large background, against which we must find powerful cuts or distributions in order to make the signal visible.

In order to proceed further, we need to examine the distributions of decay products. In figures 4 and 5 we present the rapidity and transverse momentum distributions. Since all particles in our final state are treated as being massless, the rapidity can be replaced by pseudorapidity. We have plotted the leptonic top decay modes only. For the hadronic

top decay, discarding the small effects of spin correlation, the light quark jet distributions are as the lepton distributions, and the missing momentum distribution is identical to the tau transverse momentum distribution.

We have also computed the rapidity difference between tau and the lepton, and found that the distribution does not behave significantly differently from the rapidity distribution of the lepton alone.

At first sight there seems little hope for signal detection. The rapidity distributions are similar, the small difference being partly due to spin correlation and partly due to the different resonance mass. The spin correlation can not be used to reduce the background since we have made the assumption that the top quark decays independently of production when generating the signal plots. Anyhow, there will be a small spin correlation effect in kinematic distributions involving the top quark decay, which can be used to constrain the coupling structure of signal and background events if we acquire a sufficient sample.

The tail of transverse momentum distribution for the background does not fall sufficiently to allow us to extract a convincing signal, especially if  $\tan\theta$  is not high enough. This is as remarked in [6, 13].

On a closer examination of the tail of tau transverse momenta for the background events, we note that this is not primarily due to off-shell  $W$  production, but due to  $W$  being produced back-to-back with the top quark at large transverse momenta. Indeed, the author has made a similar plot using the 'narrow width approximation' for the  $W$  and the difference between this and figure 5c is small. At a more analytical level too, it is easy to see that the off-shell effect is smaller than the kinematic effect of back-to-back production.

As noted earlier, there is an 'isotropic' component in the background production cross section (9) which makes the background even more prone to this back-to-back production than the signal. Having said that, we see that at large transverse momenta, the signal distributions of figures 5a, b also exhibit 'dips' in missing transverse momenta at high energies corresponding to the back-to-back production.

Such events are simpler to deal with than the 'down-the-beam-pipe' type events, since in this case the hadronic top quark decay can be used to reconstruct the top quark mass, giving us more control over the signal distributions.

Let us proceed as follows. Firstly, we remove events where tau and missing transverse momentum are not back-to-back, viz  $\cos\theta_{miss} < -0.2$  where  $\theta$  is the azimuthal angle. Secondly, out of the events which survive the above requirement, we remove events where, in the leptonic case, a top quark remnant, either the bottom quark or the lepton, is harder than either the tau or the missing transverse momentum. In the hadronic case, we can proceed similarly, imposing some requirement on the reconstructed top quark (or a remnant) transverse momentum against either the tau or the missing transverse momentum. As default, we adopt  $p_T(t)$  as the momentum cut-off. Thirdly, we make cuts on the tau and the missing transverse momentum, either by an explicit cut or by a plot of the cross section against  $p_T^{\text{cut}}$ .

As for the detector cuts, for the leptonic decay mode of the top quark, the only requirement is on the tau and the missing transverse momentum. This will also help eliminate the reducible background, for example, from top pair production. We tentatively set this at 50 GeV. The final transverse momentum cut mentioned above will alter this minimum value at a later stage in the analysis. We also require the tau rapidity to be between  $-2.5$  and  $+2.5$ , although this may be redundant after the transverse momentum cuts.

For the hadronic decay mode of the top quark we require all top decay products to have rapidity between  $-1.5$  and  $+1.5$ , in addition to the transverse momentum requirement above.

To summarise, the cuts are:

$$m_{\text{miss}} < p_T^{\text{cut}} = 2; \quad (11)$$

$$m_{\text{in}}(p_T(\ell); E_T^{\ell}) > \max(50 \text{ GeV}; p_T(b); p_T(t)); \quad (12)$$

$$j(\ell) < 2.5 \quad (13)$$

for the leptonic decay of the top quark, and

$$m_{\text{miss}} < p_T^{\text{cut}} = 2; \quad (14)$$

$$m_{\text{in}}(p_T(\ell); E_T^{\ell}) > \max(50 \text{ GeV}; p_T(t)); \quad (15)$$

$$j(\ell) < 2.5; \quad (16)$$

$$\max(j(b); j(q); j(\bar{q})) < 1.5 \quad (17)$$

for the hadronic decay of the top quark.

The resulting  $p_T(\ell)$  and  $E_T^{\ell}$  distributions are used to determine the optimum transverse momentum cut procedure.

The result is shown in tables 2 and 3.

The cuts are not optimised, and it is possible that the signal against background ratio can be improved without reducing the absolute rate too much. In any case, it is likely that the hadronic decay of the top quark offers a far greater chance of signal resolution, even though there is a significant loss of top remnants near the beam pipe. The improved background reduction is because of the absence of the neutrino from the decay of the top quark, allowing us to know the transverse momentum of the tau neutrino. Let us concentrate on the hadronic decay from here on.

In figure 6 we show the tau transverse momentum distribution for the background events, after cuts, before the final transverse momentum cut. The missing transverse momentum  $E_T^{\ell}$ , which we do not plot here, should have the same profile neglecting the spin correlation effects, but in practice the large integration error prevents this coincidence to materialise in our simulation.

Comparing figures 5 and 6 we see that rather than to keep  $p_T^{\text{cut}}$  as a free parameter as one would do in an experimental analysis, an easy way to simulate the effect of transverse momentum cuts is to impose cuts at 100 GeV on both tau and missing transverse momenta. The numerical integration for the background becomes very unstable at this value and renders higher cuts impractical in our simulation.

The optimisation of cuts can be achieved by balancing between keeping the production of the bosons  $H$  and  $W$  at low transverse momenta via the cuts described above for example, and the final cuts on, or the distribution of, the tau and missing transverse momenta. As we lower the transverse momenta of the bosons we also lower the transverse momentum of the top quark. Since we can not present a full simulation of top quark identification near the beam directions we do not consider it worthwhile speculating further into this, until we can utilise the full simulation.

Table 4 shows the result after the final cuts.

The cut is very effective at large  $M_H$ , where it is clear that larger values of  $p_T^{\text{cut}}$  would allow lower values of  $\tan\beta$  to be probed. This can be easily achieved in practice

by plotting the cross section after cuts against  $p_T^{\text{cut}}$ . The signal will show a bump in the distribution, which can be confused as due to  $H^0$  rather than statistical fluctuation by tau polarisation and spin correlation analyses.

For the intermediate values of  $\tan\beta$  we can extrapolate the figures by the known dependence of the cross section on  $\tan\beta$ . At  $M_{H^0} = 200$  GeV, where the transverse momentum cut is least effective, the signal-to-background ratio becomes 1:1 at  $\tan\beta = 2.5$ . Given the LHC integrated luminosity of  $100 \text{ fb}^{-1}$  for the high luminosity option, this corresponds to observing 35 events per year.

For large values of  $M_{H^0}$ , say masses higher than 500 GeV, the transverse momentum cut becomes very effective at reducing the background, but we must deal with the exponentially falling cross section (see figure 3). As an example, at  $M_{H^0} = 1$  TeV, applying the same cuts as above but setting  $p_T^{\text{cut}} = 300$  GeV, we obtain a cross section of  $0.00168 \text{ fb}$  at  $\tan\beta = 1.5$ . The numerical integration for the background is very unstable, but we consider it negligible. We find that in order to observe one event per year at the integrated luminosity of  $100 \text{ fb}^{-1}$ ,  $\tan\beta$  must be greater than 3.7.

We note that at such high values of  $M_{H^0}$ , the  $b\bar{b}$  decay mode becomes relatively clean, as what we observe will be  $b$  and  $t\bar{t}$  jets back-to-back with transverse momenta of about 500 GeV each. In the  $t\bar{b}$  decay mode too, the signal will be spectacular, with the hard tau and the missing momentum pointed back to back. Presumably the requirement of top identification becomes less important here, and the minimum  $\tan\beta$  can be lowered significantly. As a conservative estimate,  $\tan\beta > 3$  is accessible in the  $t\bar{b}$  decay mode of  $H^0$  for  $M_{H^0}$  between 200 GeV and 1 TeV.

For smaller values of  $M_{H^0}$ , the transverse momentum cut becomes less effective, we must impose stricter preliminary cuts, and the analysis becomes complex. On the other hand, this range involves kinematic suppression on the  $t\bar{b}$  decay mode of  $H^0$ , and the branching ratio into  $t\bar{b}$  becomes greater. As an added bonus, the  $W^{\pm}h^0$  mode kicks in at low  $\tan\beta$  where the  $t\bar{b}$  channel becomes the least effective, which is easy to handle by imposing  $b$  vertex tagging on  $h^0$ !  $b\bar{b}$  since we will hopefully know the  $h^0$  mass at an early stage in LHC operation.

## 5 Conclusions

We have discussed the search for the charged Higgs bosons  $H^{\pm}$  of the Two Higgs Doublet Model, inherent for example in MSSM, through the  $t\bar{b}$  decay mode at LHC through the 'tb fusion' production channel.

We have found that after a combination of kinematic cuts, there is a vast parameter space in which  $H^{\pm}$  can be discovered, which have previously been thought inaccessible at LHC.

For  $H^{\pm}$  masses heavier than 200 GeV, up to say 1 TeV, they can be discovered for  $\tan\beta > 3$ . This is without the optimisation of cuts.

Provided we neglect the other decay modes which are model dependent, the cross section is roughly proportional to  $\tan^2\beta$ , which implies that if we improve the procedure merely by fourfold, which is not unrealistic, the minimum  $\tan\beta$  that can be probed falls to 1.5, which is below the maximum  $\tan\beta$  probed so far at LEP 2 assuming MSSM.

The signal thus discovered can be confirmed by analysing the tau polarisation and spin correlations.

The plots of the tau and the missing transverse momenta indicate that the  $H$  mass can be evaluated to some degree from the signal distribution provided there is large enough sample. At least before cuts, the  $p_T$  distributions of the tau and the missing transverse momenta are independent of  $\tan\beta$ , allowing one to reconstruct  $M_H$ . The total cross section, being proportional to  $\tan^2\beta$ , is then a good measure of  $\tan\beta$ . The spin correlations involving the top quark decay products can be used to constrain this measurement.

The model dependent region near and below the tb decay threshold, at  $M_H < 200$  GeV, has not been treated in detail. A full study of this region is desired, assuming  $M_{ssm}$ , or otherwise.

We only considered the irreducible background to this process. The reducible background includes top pair production and  $W + jets$  production. The second one is presumably removable by imposing the top selection and as long as we impose some jet profile criterion in the selection (so as to filter out soft multi-jets), it is at higher order in  $\alpha_s$  anyhow. The top pair background is only significant if one of the bottom quarks from top decay escapes in the beam pipe. Although the cross section for this may not be negligible, this is hardly likely to lead to large tau and missing transverse momenta, as is the  $W + jets$  background, and should be negligible in our analysis.

We did not consider the supersymmetric background, notably the  $2+2$  sbottom + neutralino production from gg fusion, with the sbottom decaying into top quark,  $W$  and neutralino. In some regions of the supersymmetric parameter space where the sbottom decays into a top quark and a chargino and the chargino decays into a  $W$  and a neutralino, such background will be large.

Once  $H$  has been discovered in this channel, the mass and the  $\tan\beta$  thus obtained can be used to optimise the signal extraction procedure for other modes, notably the dominant tb decay, leading to a better understanding of the two-doublet Higgs sector.

Our analysis is sensitive to top quark identification near the beam direction, especially in the hadronic channel. This needs to be studied with full jet and detector simulations, leading to the optimisation of the signal extraction procedure, before the exact discovery contour can be elucidated. We note that as long as top quark is identified as such, we do not require much more information, other than the guarantee that there is no other source of missing transverse momentum, for our analysis. In fact, this guarantee may be sufficient on its own when using our procedure of selecting high transverse momentum decay products from charged bosons produced at low transverse momentum. The effect on reducible background of relaxing the top quark identification requirement may thus be worth analysing.

## Acknowledgements

I thank Stefano Moretti for advice, discussions and for reading the manuscript, and Bryan Webber for his guidance through my Ph.D. at Cambridge.

## References

- [1] F. Richard, preprint LAL 98-74, hep-ex/9810045, talk given at ZuoZ Summer School on Hidden Symmetries and Higgs Phenomena, ZuoZ, Switzerland, 16-22 August 1998.

[2] The ALEPH collaboration, *Phys. Lett. B* 429 (1998) 169.

[3] See, for example, S. Moretti and K. Odagiri, *J. Phys. G* 23 (1997) 537 and references therein.

[4] M. Spira, talk presented at "Physics at Run II: Workshop on Supersymmetry", Batavia, IL, 19-21 November 1998, preprint DESY 98-159.

[5] A. Krause, T. Plehn, M. Spira and P.M. Zerwas, *Nucl. Phys. B* 519 (1988) 85; V. Barger, R.J.N. Phillips and D.P. Roy, *Phys. Lett. B* 324 (1994) 236; M. Guchait and D.P. Roy, *Phys. Rev. D* 55 (1997) 7263.

[6] J.F. Gunion, H.E. Haber, G.L. Kane and S. Dawson, 'The Higgs Hunter's Guide' (Addison-Wesley, Reading MA, 1990).

[7] B.K. Bullock, K. Hagiwara and A.D. Martin, *Phys. Rev. Lett.* 67 (1991) 3055.

[8] A.D. Martin, R.G. Roberts, W.J. Stirling, R.S. Thorne, *Phys. Lett. B* 443 (1998) 301.

[9] Particle Data Group, 'Review of particle physics', *Eur. Phys. J. C* 3 (1998) 1.

[10] CMS Technical Proposal, CERN/LHC/94-43 LHCC/P1 (December 1994);  
ATLAS Technical Proposal, CERN/LHC/94-43 LHCC/P2 (December 1994).

[11] G.P. Lepage, *Jour. Comp. Phys.* 27, (1978) 192.

[12] J.A.M. Vermaasen, 'The Symbolic Manipulation Program FORM', Computer Algebra Netherland, Amsterdam 1991.

[13] J.F. Gunion, H.E. Haber, F.E. Paige, W.K. Tung and S.S.D. Willenbrock, *Nucl. Phys. B* 294 (1987) 621.

[14] R.K. Ellis and S. Parke, *Phys. Rev. D* 46 (1992) 3785.

## Table captions

Table 1: Signal rates for some typical values of  $M_H$  and  $\tan\beta$ , and the 'isotropic' and 'scalar' background components.

Table 2: Signal and background rates in the hadronic decay mode of the top quark, after the selection cuts, before the final transverse momentum cut.

Table 3: Signal and background rates in the hadronic decay mode of the top quark, after the selection cuts, before the final transverse momentum cut.

Table 4: Signal and background rates in the hadronic decay mode of the top quark, after the final transverse momentum cut, with  $p_T^{\text{cut}} = 100 \text{ GeV}$ .

## Figure captions

Figure 1: Lowest order Feynman graphs for process (1). Top and  $H \rightarrow$  decays are omitted for simplicity.

Figure 2: (a { top) The tree level branching ratio of  $H \rightarrow$  in the large mass limit,  $M_H^2 / m_t^2$ , as functions of  $\tan \beta$ . (b { bottom) The overall tree level  $\tan \beta$  dependence of production and  $H \rightarrow$  decay, in the large mass limit of  $H \rightarrow$  .

Figure 3: The total cross section in picobarns at LHC for  $gb \rightarrow tH \rightarrow$ , as a function of  $M_H$ .  $bg \rightarrow tH \rightarrow$  and the charge conjugate processes are not included. Cross section must be multiplied by 4, the  $\tan \beta$  dependence of (8) and the kinematical suppression of (5).

Figure 4: Rapidity distributions for signal and background at LHC energy.  $bg$  initial state is not included. Rapidity is positive along the direction of the  $g$  initial state parton. Normalisation is to unity. Lines were used instead of histograms for the sake of visibility. Binning width is 1. (a { top) Signal events at  $M_H = 200$  GeV. (b { middle) Signal events at  $M_H = 500$  GeV. (c { bottom) Background.

Figure 5: Transverse momentum distributions for signal and background at LHC energy. Normalisation is to unity. Lines were used instead of histograms for the sake of visibility. Binning width is 50 GeV. (a { top) Signal events at  $M_H = 200$  GeV. (b { middle) Signal events at  $M_H = 500$  GeV. (c { bottom) Background.

Figure 6: Background transverse momentum distribution after the selection cuts, before the final transverse momentum cut. Normalisation is to unity. See text for the cuts.

| $M_H$ (GeV) | $\tan \beta$ | (fb)  |
|-------------|--------------|-------|
| bg ! tH     | ! t          |       |
| 200         | 1.5          | 4.78  |
| 200         | 30           | 1530  |
| 500         | 1.5          | 0.139 |
| 500         | 30           | 52.1  |
| bg ! tW     | ! t          |       |
| total       |              | 13260 |
| 'isotropic' |              | 6650  |
| 'scalar'    |              | 6610  |

Table 1

| $M_H$ (GeV)   | $\tan \beta$ | $\sigma (fb)$ |
|---------------|--------------|---------------|
| 200           | 1.5          | 0.252         |
| 200           | 30           | 81.0          |
| 500           | 1.5          | 0.0205        |
| 500           | 30           | 7.69          |
| $\sigma (fb)$ |              | 2.4           |

Table 2

| $M_H$ (GeV)                 | $\tan \beta$ | $\sigma (fb)$ |
|-----------------------------|--------------|---------------|
| 200                         | 1.5          | 0.388         |
| 200                         | 30           | 124           |
| 500                         | 1.5          | 0.0240        |
| 500                         | 30           | 9.00          |
| $\sigma_{bg} + \sigma_{tH}$ |              | 372           |

Table 3

| M <sub>H</sub> (GeV) | tan  | (fb)   |
|----------------------|------|--------|
| bg ! tH ! t          |      |        |
| 200                  | 1.5  | 0.123  |
| 200                  | 30   | 39.4   |
| 500                  | 1.5  | 0.0177 |
| 500                  | 30   | 6.659  |
| bg ! tW ! t          |      |        |
|                      | 0.35 | 0.09   |

Table 4

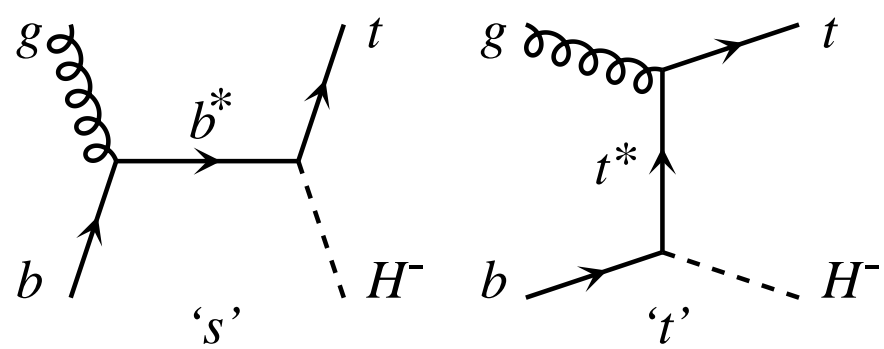


Figure 1

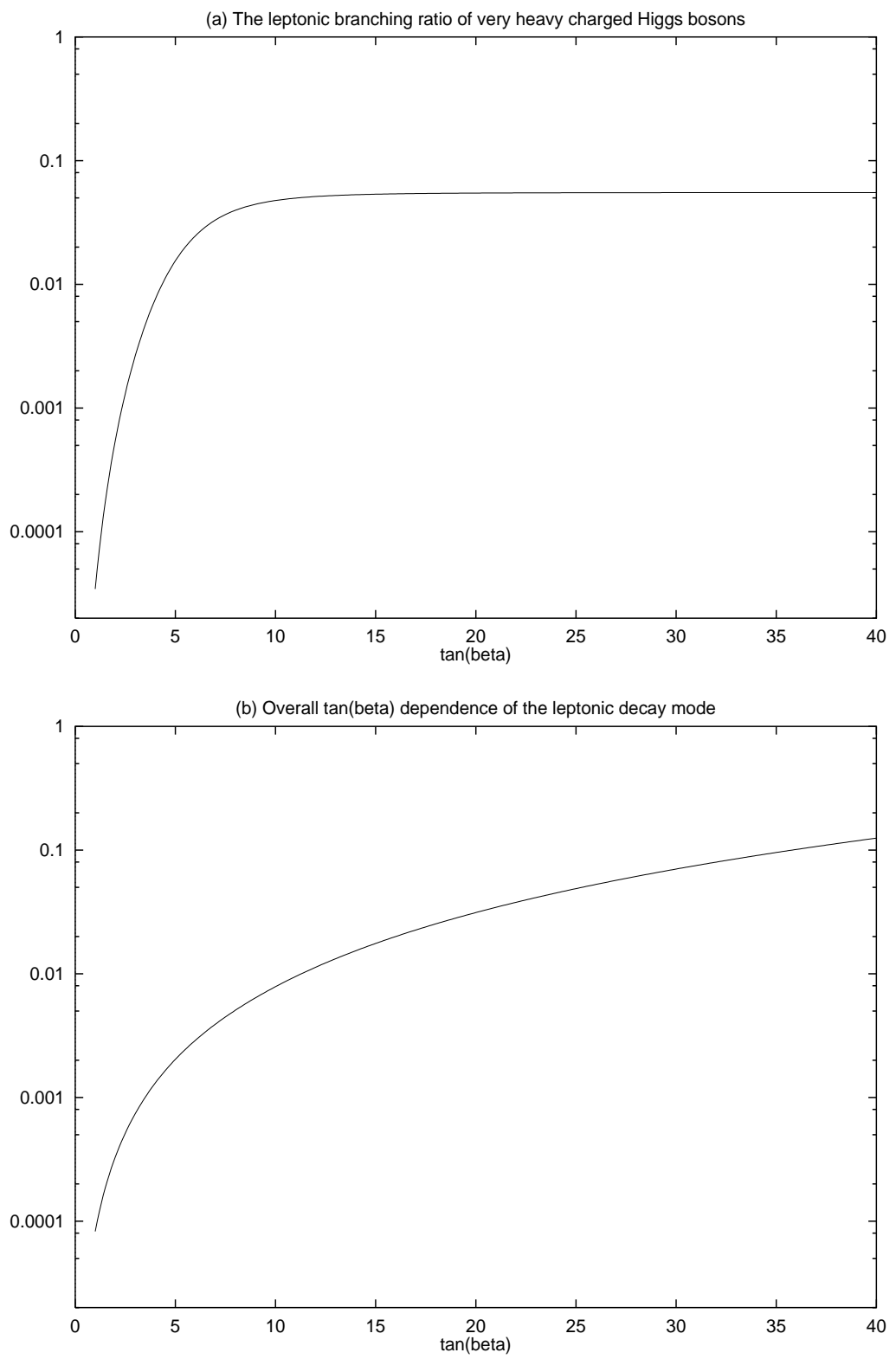


Figure 2

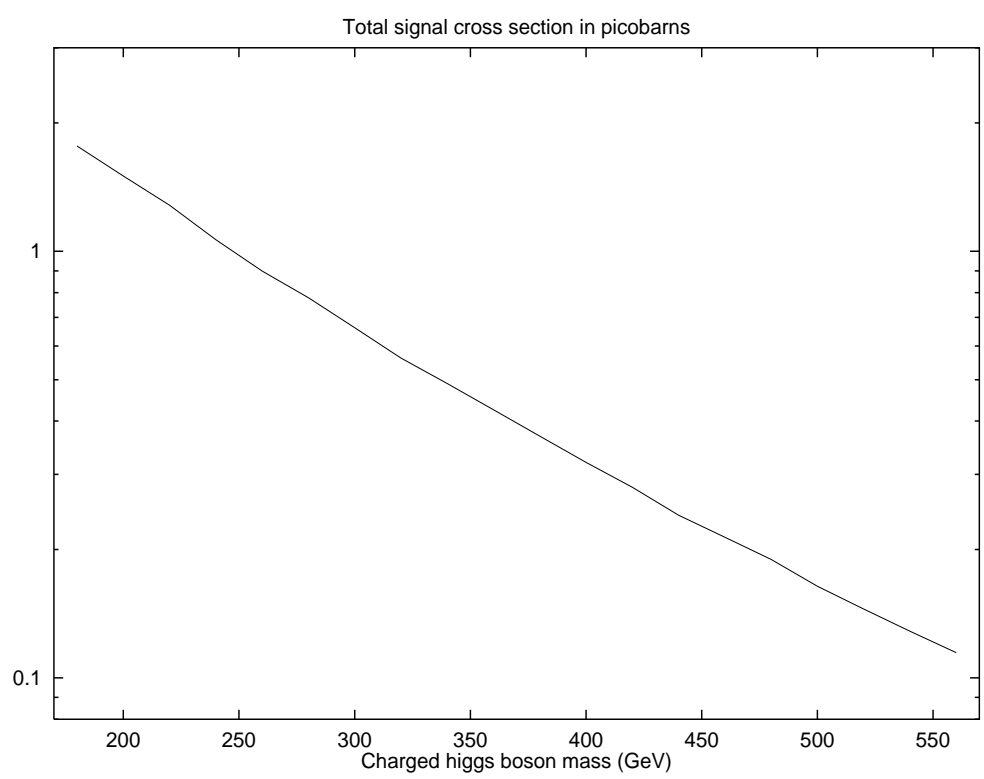


Figure 3

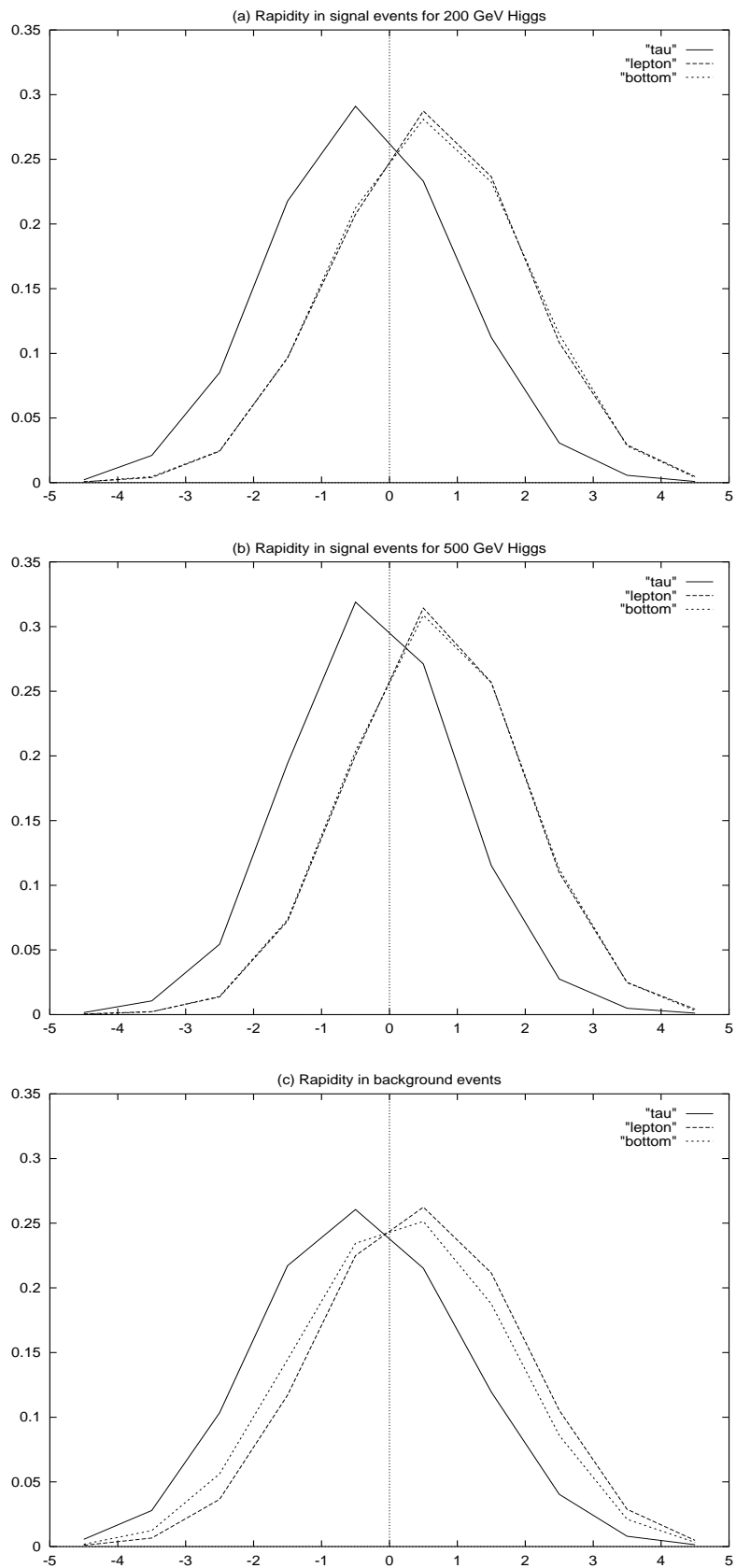


Figure 4

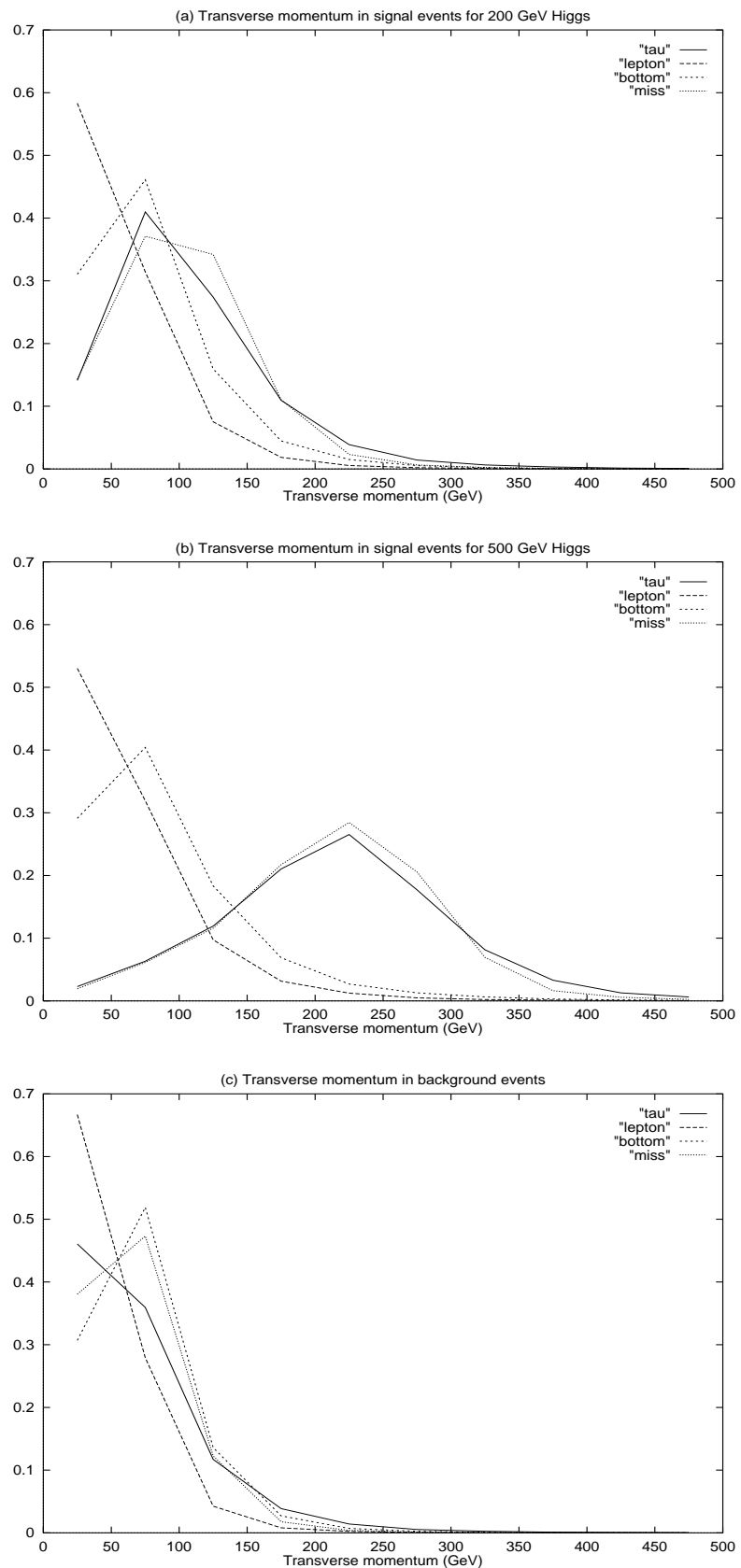


Figure 5

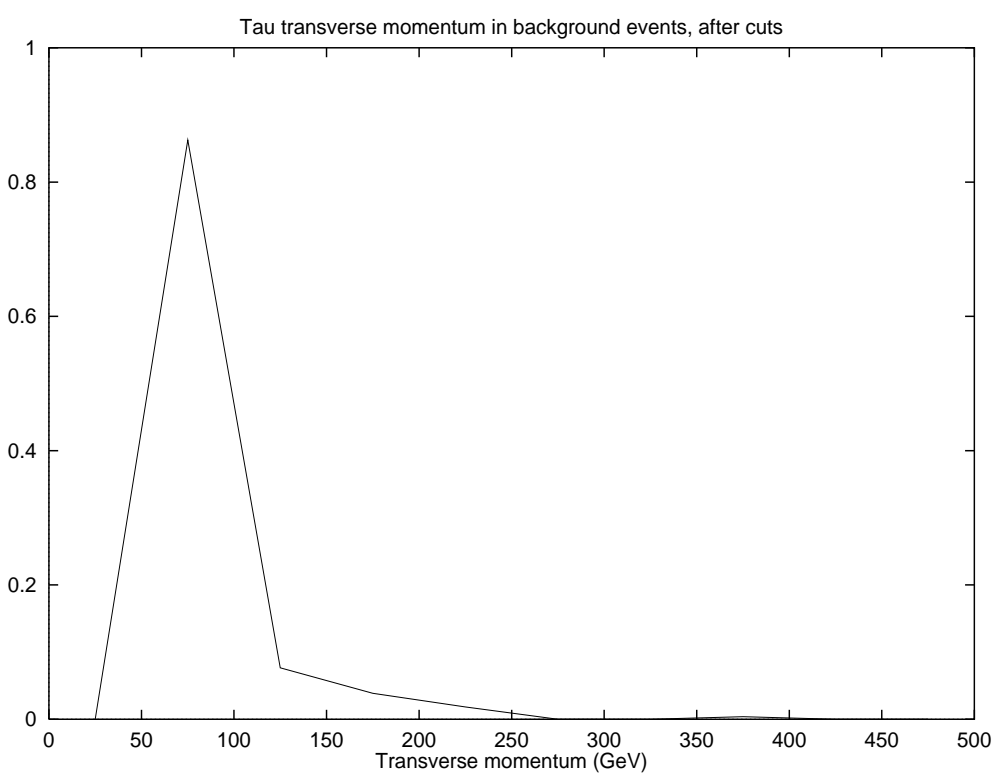


Figure 6